Editors' Suggestion

Analytical expression of a finite, long, conical canted-cosine-theta coil for particle collider interaction regions

Ye Yang,* Shlomo Caspi, and Lucas Brouwer

Lawrence Berkeley National Laboratory (LBNL), One Cyclotron Road, Berkeley, California 94720, USA

(Received 28 May 2025; accepted 10 October 2025; published 27 October 2025)

Magnets in the accelerator interaction region (IR) present significant challenges because of high field requirements and limited available space. Conical-shaped magnets offer advantages in these environments by allowing closer placement to the interaction point while maintaining clearance from synchrotron radiation. Interestingly, numerical studies have shown that conical canted-cosine-theta (CCT) designs produce a constant field distribution along the axial direction in the IR quadrupoles for the Electron-Ion Collider (EIC) at Brookhaven National Laboratory. However, the field harmonics generated by conical CCT windings are not yet fully understood. This paper presents an analytical approach to describe the magnetic field produced by a conical surface current and proposes a method for designing conical CCT magnets for accelerator applications. First, we begin with a surface current sheet having a general cosine-theta distribution in spherical coordinates and solve the vector potential using the Green's function. The magnetic fields generated by the conical current sheet are expressed using associated Legendre polynomials. These results are then related to circular field harmonics and integral field harmonics for designing a coil that produces a pure multipole field. Next, a single layer of the conical CCT winding path is produced based on the cosine-theta current distribution. Finally, the magnetic field quality of dipole and quadrupole conical CCT coils with multiple layers is verified using the Biot-Savart law.

DOI: 10.1103/n8tc-1334

I. INTRODUCTION

Magnets located in the collider interaction region (IR) are particularly challenging to design because they must provide a high magnetic field and good field quality within a very limited space, while also minimizing magnetic crosstalk between nearby apertures. To achieve high luminosity, particle beams are tightly focused to nanometer-scale spot sizes at the interaction point (IP). In many designs, the final focusing quadrupoles are positioned several meters from the IP with very small crossing angles, which requires placing the quadrupoles extremely close to each other [1,2]. This inevitably leads to significant magnetic crosstalk between apertures. While an iron yoke can help shield fringe fields, its effectiveness is limited by iron saturation at high fields. Shielding coils, such as those employed in the SuperKEKB IR superconducting magnets, offer a promising alternative option. However, designing these coils is complicated by the fact that the crosstalk induced field harmonics vary considerably along the axial direction [3–5]. Moreover, in designs like that of the Electron-Ion Collider (EIC), where synchrotron radiation from beam separation must pass through the magnets, both the beam pipes and the coils are needed to be tapered to accommodate this constraint.

Brookhaven National Laboratory (BNL) previously developed conical quadrupole coils for the HERA interaction region (IR) using a nested serpentine winding pattern fabricated with direct winding technology [6,7]. It was observed that the quadrupole field gradient naturally decreases along the axial direction because of the change of radius, requiring more turns near the major radius to compensate for the reduced field. Currently, a conical canted-cosine-theta (CCT) coil, also manufactured via direct winding, is being proposed for the EIC IR quadrupole magnets as an alternative to traditional cosine-theta coils. The CCT concept, first introduced in the 1970s, offers several benefits, including improved stress management, simplified fabrication, and the elimination of integral field errors [8,9]. It also allows flexible harmonic combinations, which can facilitate the design of shielding coils. Interestingly, the conical CCT winding exhibits a unique behavior: the quadrupole field gradient does not significantly decrease along the axial direction. This characteristic highlights the great potential of using CCT technology for

*Contact author: yeyang@lbl.gov

Published by the American Physical Society under the terms of the Creative Commons Attribution 4.0 International license. Further distribution of this work must maintain attribution to the author(s) and the published article's title, journal citation, and DOI.

final focusing quadrupole magnets, particularly from the perspective of field integration.

For the EIC IR quadrupole coils, the conical CCT winding path has been generated numerically by using the formula originally developed for cylindrical CCT windings. This approach requires parameter tuning to compensate for variations in the quadrupole component along the conical geometry. It has also been observed that such conical quadrupole windings inherently produce a skew octupole component [10,11]. To the best of the authors' knowledge, an analytical explanation that directly relates the conical CCT winding path to the resulting field harmonics has not yet been developed.

In addition to IR magnets, conical-shaped multipole magnets have also been utilized in medical accelerators. In the latest rotating gantry developed by the National Institutes for Quantum Science and Technology and Toshiba, normal-conducting scanning magnets were designed with a conical geometry to accommodate the large beam acceptance required downstream of the gantry [12–14]. The conical CCT concept is currently being considered as a second-generation solution for scanning magnets in cancer therapy [15]. Therefore, developing a conical CCT winding path directly related to the desired field harmonics is valuable for a wide range of applications.

In a previous study, we investigated the magnetic properties of a dipole conical CCT magnet [16]. However, the method for generating the CCT winding path with control of high-order harmonics was not provided. In this paper, we present an analytical framework for a conical CCT superconducting magnet. In Sec. II, we derive the vector potential and magnetic fields using the Green's function in spherical coordinates, assuming a conical surface carrying a cosine-theta current density. The derived magnetic fields are then related to circular field harmonics for practical applications. Section III details the derivation of a conical CCT winding path in spherical coordinates and validates the conical CCT coil design using the Biot-Savart law. Finally, the conclusions are summarized in Sec. IV.

II. MAGNETIC FIELD FOR A CONICAL CURRENT SHEET

A. Spherical coordinate

Figure 1 depicts the conical shape subtracted from a sphere in a spherical coordinate system where $x = r\sin\theta\cos\phi$, $y = r\sin\theta\sin\phi$, and $z = r\cos\theta$ (r, spherical radius; θ, zenithal angle; ϕ, azimuthal angle). Taking advantage of the spherical coordinate system, a cone can be simply represented by the parameters of the minor, major spherical radii, a and b, and the zenithal angle. Using the zenith angle and spherical radius, the height h, minor conical radius ρ_0, and major conical radius ρ_1 of the cone can be determined as

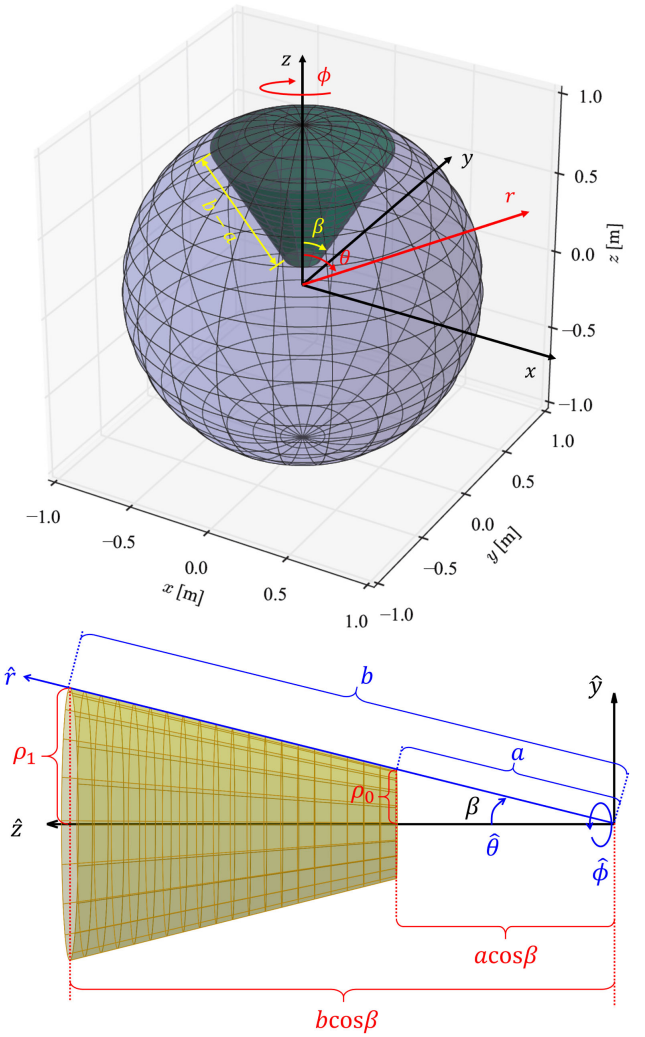


FIG. 1. Extraction of a conical shape from spherical coordinates (r, θ, ϕ) and a projection of the cone into the y-z plane.

$$\begin{aligned} h &= (b-a)\cos\theta, \\ \rho_0 &= a\sin\theta, \\ \rho_1 &= b\sin\theta \end{aligned} \tag{1}$$

With standard scale factors of $h_r = 1$, $h_\theta = r$, and $h_\phi = r\sin\theta$, we can get the expression of the curl and divergence in the spherical coordinate system for producing the magnetic field. The curl of a vector potential $\vec{A} = A_r\hat{r} + A_\theta\hat{\theta} + A_\phi\hat{\phi}$ related to the magnetic fields is obtained as

$$\begin{aligned} \nabla\times\vec{A} = &\frac{1}{r\sin\theta}\left\{\frac{\partial(A_\phi\sin\theta)}{\partial\theta} - \frac{\partial A_\theta}{\partial\phi}\right\}\hat{r} \\ &+ \left\{\frac{1}{r\sin\theta}\frac{\partial A_r}{\partial\phi} - \frac{1}{r}\frac{\partial(rA_\phi)}{\partial r}\right\}\hat{\theta} \\ &+ \left\{\frac{1}{r}\frac{\partial(rA_\theta)}{\partial r} - \frac{1}{r}\frac{\partial A_r}{\partial\theta}\right\}\hat{\phi}. \end{aligned} \tag{2}$$

Because the divergence of a current density is zero everywhere according to the electromagnetic theory, the divergence of a current density vector $\vec{J} = J_r\hat{r} + J_\theta\hat{\theta} + J_\phi\hat{\phi}$ must satisfy with

$$\nabla \cdot \vec{J} = \frac{1}{r^2}\frac{\partial}{\partial r}(r^2 J_r) + \frac{1}{r\sin\theta}\frac{\partial}{\partial\theta}(\sin\theta J_\theta) + \frac{1}{r\sin\theta}\frac{\partial J_\phi}{\partial\phi} = 0. \tag{3}$$

It is easy to translate the field components from the spherical coordinate system to the other coordinate system using the unit vectors. The unit vectors related to the one in the Cartesian coordinate system is given by

$$\begin{aligned}\hat{r} &= \sin\theta\cos\phi\hat{x} + \sin\theta\sin\phi\hat{y} + \cos\theta\hat{z}\\ \hat{\theta} &= \cos\theta\cos\phi\hat{x} + \cos\theta\sin\phi\hat{y} - \sin\theta\hat{z}\\ \hat{\phi} &= -\sin\phi\hat{x} + \cos\phi\hat{y}.\end{aligned} \tag{4}$$

B. Vector potential

Magnets are typically treated as infinitely long along the axial axis, and the magnetic fields are derived from the Laplace equation and its boundary conditions in two dimensions for accelerator magnets. However, approaching the conical shape in spherical coordinates is challenging because of the singularity at the origin of the spherical coordinate system. To address this challenge, we utilize the Green's function to solve the magnetic problem.

The solution of the Poisson equation $\nabla^2\vec{A} = -\mu_0\vec{J}$ is given by [17]

$$\vec{A}(\vec{x}) = \frac{\mu_0}{4\pi}\int\frac{\vec{J}(\vec{x}')}{|\vec{x}-\vec{x}'|}d^3x', \tag{5}$$

where $\vec{J}$, $\vec{x}$, and $\vec{x}'$ are the vector of the current density, observed point, and current source point, respectively. The inverse of the distance between the source and observed point can be replaced by the Green's function so that the vector potential of a current source at the constant conical angle can be rewritten as

$$\vec{A}(\vec{x}) = \frac{\mu_0}{4\pi}\iiint\vec{J}(\vec{x}')G(\vec{x},\vec{x}')\frac{\delta(\theta'-\theta_0)}{h_\theta}h_r h_\theta h_\phi dr'd\theta'd\phi', \tag{6}$$

where $\delta(\theta'-\theta_0)$ is the delta function that constrains the current density on a constant surface where $\theta' = \theta_0$. $G(\vec{x},\vec{x}')$ is the Green's function expressed in the spherical coordinate system as

$$\begin{aligned}G(\vec{x},\vec{x}') &= \frac{1}{|\vec{x}-\vec{x}'|}\\ &= 4\pi\sum_{l=0}^{\infty}\sum_{m=-l}^{l}\frac{1}{2l+1}\frac{r_<^l}{r_>^{l+1}}Y_{lm}^*(\theta',\phi')Y_{lm}(\theta,\phi),\end{aligned} \tag{7}$$

where $r_>(r_<)$ is the larger (smaller) of observed point $|\vec{x}|$ and source point $|\vec{x}'|$. If the radius of source current is smaller than the observed point ($r' < r$), the $r_<$ and $r_>$ are equal to r' and r, respectively, and vice versa. $Y_{lm}(\theta,\phi)$ and $Y_{lm}^*(\theta',\phi')$ are the spherical harmonics functions and its complex conjugation, which represent the field harmonics with the orders of l and m. The spherical harmonics function is defined as

$$\begin{aligned}Y_l^m(\theta,\phi) &= \sqrt{\frac{2l+1}{4\pi}\frac{(l-m)!}{(l+m)!}}P_l^m(\cos\theta)e^{im\phi}\\ &= \sqrt{\frac{1}{4\pi}}\bar{P}_l^m(\cos\theta)e^{im\phi},\end{aligned} \tag{8}$$

where $P_l^m(\cos\theta)$ and $\bar{P}_l^m(\cos\theta)$ are the associated Legendre functions (ALFs) and fully normalized ALFs, respectively [18].

In this study, we define a conical source current is constrained on a surface with a constant conical angle of $\theta' = \beta$, minor and major spherical radius of a and b. In terms of the current density, as the cone also has a circular bore at the cross section along the axial axis, we initially assume the current density has a typical cosine-theta distribution along the axial direction as

$$\begin{aligned}\vec{J} &= J_n\cos(n\phi')\hat{z}\\ &= J_n\sin\beta\cos(n\phi')\hat{r} - J_n\cos\beta\cos(n\phi')\hat{\theta},\end{aligned} \tag{9}$$

where J_n is the constant current density corresponding to each order of the harmonics. According to Eq. (3), the divergence of the assumed current density is also zero by feeding the current in the zenithal direction. Noting that we still treat the current density as a pseudo-two-dimensional problem since there is no azimuthal component to constrain the current in the region of $a \le r' \le b$. Inserting Eqs. (7)–(9) into Eq. (6), the radial and zenithal components of vector potential can be rewritten as

$$\begin{pmatrix}A_r\\ A_\theta\end{pmatrix} = \frac{\mu_0 J_n}{4\pi}\begin{pmatrix}\sin\beta\cos\beta\\ -\sin^2\beta\end{pmatrix}\mathrm{Re}\left\{\sum_{l=0}^{\infty}\sum_{m=-l}^{l}\frac{(l-m)!}{(l+m)!}P_l^m(\cos\beta)P_l^m(\cos\theta)e^{im\phi}\int_0^{2\pi}e^{i(n-m)\phi'}d\phi'\int_a^b\frac{r_<^l}{r_>^{l+1}}r'dr'\right\}. \tag{10}$$

According to the orthogonality relations, the integral over the azimuthal direction is given by

$$\int_0^{2\pi} e^{i(n-m)\phi'} d\phi' = \begin{cases} 2\pi, & m = n \\ 0, & m \neq n \end{cases}. \tag{11}$$

It can be seen that all the terms that $m \neq n$ are removed, and only the terms that $m = n$ remain in the summation.

In terms of the integral over the radial direction, the integral is solved by separating it into the three regions: $(0 < r < a)$, $(a \leq r \leq b)$, and $(r > b)$. Furthermore, we define the radial integrals divided by r as a function of $R_l(r)$ to simplify the calculation for the magnetic fields. The function $R_l(r)$ in each region is calculated as

$$\begin{aligned} R_l(0 < r < a) &= \frac{1}{r}\int_a^b \frac{r^l}{r'^l} dr' \\ &= \begin{cases} \ln(\frac{b}{a}), & l = 1 \\ \frac{1}{l-1}[(\frac{r}{a})^{l-1} - (\frac{r}{b})^{l-1}], & l \neq 1 \end{cases}, \end{aligned} \tag{12}$$

$$\begin{aligned} R_l(a \leq r \leq b) &= \frac{1}{r}\int_a^r \frac{r'^{l+1}}{r^{l+1}} dr' + \frac{1}{r}\int_r^b \frac{r^l}{r'^l} dr' \\ &= \frac{1}{l+2}\left[1 - \left(\frac{a}{r}\right)^{l+2}\right] \\ &\quad + \begin{cases} \ln(\frac{b}{r}), & l = 1 \\ \frac{1}{l-1}[1 - (\frac{r}{b})^{l-1}], & l \neq 1 \end{cases}, \end{aligned} \tag{13}$$

and

$$R_l(r > b) = \frac{1}{r}\int_a^b \frac{r'^{l+1}}{r^{l+1}} dr' = \frac{1}{l+2}\left[\left(\frac{b}{r}\right)^{l+2} - \left(\frac{a}{r}\right)^{l+2}\right]. \tag{14}$$

In final, the radial and zenithal components of vector potential can be simplified to the following expression:

$$\begin{aligned} A_r(r,\theta,\phi) &= \frac{\mu_0 J_n}{2} r \sin\beta\cos\beta\cos(n\phi) \\ &\quad \times \sum_{l=n}^{\infty} \frac{(l-n)!}{(l+n)!} P_l^n(\cos\beta) P_l^n(\cos\theta) R_l(r), \end{aligned} \tag{15}$$

$$\begin{aligned} A_\theta(r,\theta,\phi) &= -\frac{\mu_0 J_n}{2} r \sin^2\beta\cos(n\phi) \\ &\quad \times \sum_{l=n}^{\infty} \frac{(l-n)!}{(l+n)!} P_l^n(\cos\beta) P_l^n(\cos\theta) R_l(r). \end{aligned} \tag{16}$$

Indeed, this expression of the vector potential contains the factorial of a non-negative integer l and n. It introduces difficulties in computing the field with high-order terms because the terms at the numerator or denominator becomes an infinite value. For conventional multipole fields, the factorial term is needed to be substituted with

$$\frac{(l-n)!}{(l+n)!} = \begin{cases} \frac{1}{(l+1)l}, & \text{dipole} \\ \frac{1}{(l+2)(l+1)l(l-1)}, & \text{quadrupole} \\ \frac{1}{(l+3)(l+2)(l+1)l(l-1)(l-2)}, & \text{sextupole} \end{cases}. \tag{17}$$

Another approach to avoid the factorial term going to infinity when using high-order terms is to employ the expression of the fully normalized ALFs [18].

C. Magnetic fields

We use $\vec{B} = \nabla \times \vec{A}$ to derive the magnetic field $\vec{B} = B_r\hat{r} + B_\theta\hat{\theta} + B_\phi\hat{\phi}$. Since only the radial and zenithal components of the vector potential exist, according to Eq. (2), the magnetic fields result in

$$\begin{aligned} B_r(r,\theta,\phi) &= -\frac{\mu_0 J_n}{2}\sin^2\beta\sin(n\phi)\sum_{l=n}^{\infty}\frac{(l-n)!}{(l+n)!}P_l^n(\cos\beta)\frac{nP_l^n(\cos\theta)}{\sin\theta}R_l(r), \\ B_\theta(r,\theta,\phi) &= -\frac{\mu_0 J_n}{2}\sin\beta\cos\beta\sin(n\phi)\sum_{l=n}^{\infty}\frac{(l-n)!}{(l+n)!}P_l^n(\cos\beta)\frac{nP_l^n(\cos\theta)}{\sin\theta}R_l(r), \\ B_\phi(r,\theta,\phi) &= -\frac{\mu_0 J_n}{2}\sin\beta\cos(n\phi)\sum_{l=n}^{\infty}\frac{(l-n)!}{(l+n)!}P_l^n(\cos\beta)\left\{\sin\beta P_l^n(\cos\theta)S_l(r) + \cos\beta\frac{\partial P_l^n(\cos\theta)}{\partial\theta}R_l(r)\right\}, \end{aligned} \tag{18}$$

where the function $S_l(r)$ is given by

$$S_l(0 < r < a) = \begin{cases} 2\ln(\frac{b}{a}), & l = 1 \\ \frac{l+1}{l-1}[(\frac{r}{a})^{l-1} - (\frac{r}{b})^{l-1}], & l \neq 1 \end{cases} \tag{19}$$

$$\begin{aligned} S_l(a \leq r \leq b) &= \frac{2}{l+2} + \frac{l}{l+2}\left(\frac{a}{r}\right)^{l+2} \\ &\quad + \begin{cases} 2\ln(\frac{b}{r}) - 1, & l = 1 \\ \frac{2}{l-1} - \frac{l+1}{l-1}(\frac{r}{b})^{l-1}, & l \neq 1 \end{cases}, \end{aligned} \tag{20}$$

and

$$S_l(r > b) = \frac{l}{l+2}\left[\left(\frac{a}{r}\right)^{l+2} - \left(\frac{b}{r}\right)^{l+2}\right], \tag{21}$$

The component B_θ has a singularity as the zenith angle (conical angle) of θ close to 0 and π, and the calculation of B_ϕ requires the derivative of the ALFs. These can be obtained by using the following recurrence properties of the ALFs:

$$\frac{nP_l^n}{\sin\theta} = -\frac{1}{2}\{P_{l+1}^{n+1} + (l-n+1)(l-n+2)P_{l+1}^{n-1}\},$$
$$\frac{\partial P_l^n}{\partial\theta} = -\frac{1}{2}\{(l+n)(l-n+1)P_l^{n-1} - P_l^{n+1}\}. \tag{22}$$

It is clear that the magnetic fields in a conical coil also exhibit a pure cosine-theta distribution at a constant zenithal angle and radius, if we ignore the three-dimensional field distribution and only focus on B_ϕ. In other words, the assumed cosine-theta current density is one of the solution to produce the multipole fields at each cross section of the cone. According to Eq. (4), the component B_θ and B_r can be decomposed to the components of B_z and B_ρ in a cylindrical coordinate system. The unwanted axial field is introduced by the conical geometry, and the axial field increases as the conical angle β increases.

In these analytic expressions, the maximum order of the ALFs, l, significantly affects the magnetic field. Figure 2 shows the field distributions along the zenith angle computed with the different maximum orders. We clearly see field oscillations when the summation is terminated at $l_{\max} = 40$, and the stabilization of the field is remarkably improved by increasing the orders until $l_{\max} = 4000$. Despite summing up the field until a high-order term, we still observe a field drop at the origin of the spherical coordinate system, introducing uncertainty in producing magnetic fields for a conical coil with a narrow angle. To mitigate this singularity, we can expand the magnetic field using circular harmonics at a reference radius far from the origin, which will be described in Sec. II D.

D. Circular field harmonics

The design of accelerator magnets and beam dynamics need the use of circular harmonics, which are helpful in connecting the magnetic fields to them. It is worth noting that circular harmonics represent the two-dimensional solution of the Laplace equation, where there is no field gradient along the axial axis. The circular harmonics do not fully represent the conical fields, since the axial field arises in the conical coil because of its conical angle β.

Despite the uncertainties associated with circular harmonics in representing the three-dimensional magnetic fields, here, we derive a solution to address the singularity mentioned in the previous section and provide relation between the current density and the multipole field for producing the conical CCT winding path. We translate the magnetic fields from the spherical coordinate system into

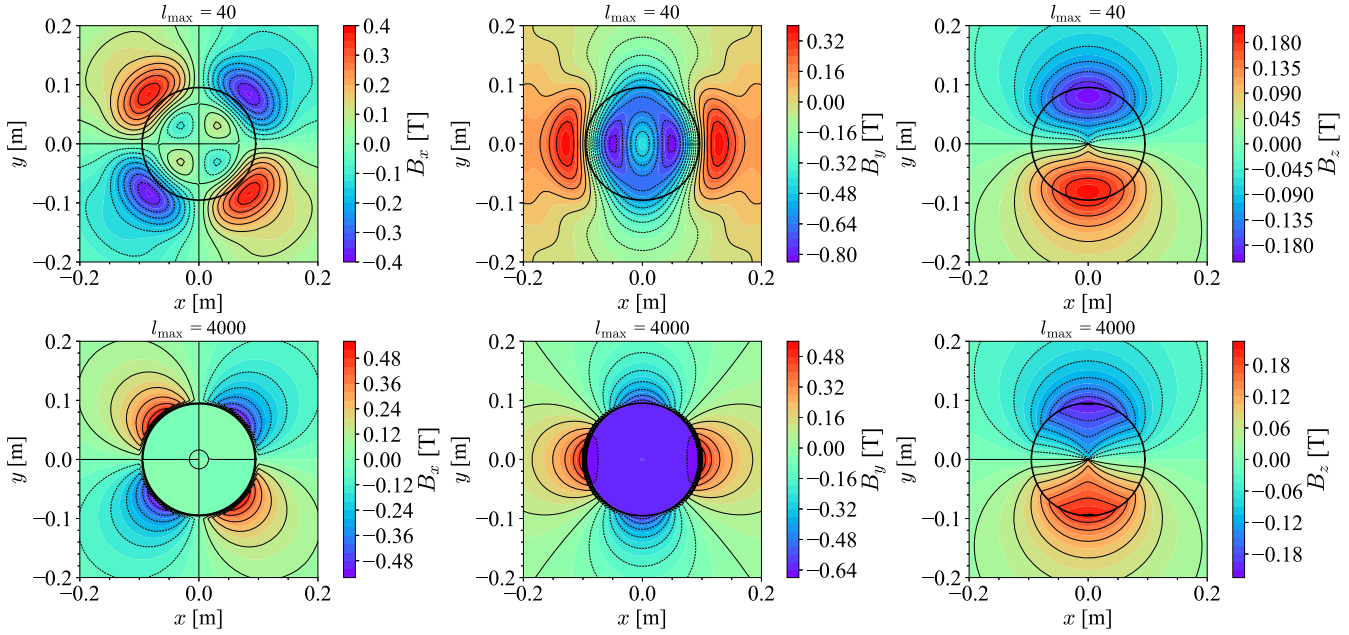


FIG. 2. The magnetic field distribution at the cone center of $(a+b)/2$. The coil parameters are $J_n = 10^6$ [A/m], $a = 100$ [mm], $b = 1000$ [mm], and $n = 1$. The upper and lower figures are calculated with the maximum order of $l_{\max} = 40$ and $l_{\max} = 4000$, respectively.

the cylindrical coordinate (ρ, z, ϕ) by using the relation of $B_\rho\hat{\rho} + B_z\hat{z} + B_\phi\hat{\phi} = B_r\hat{r} + B_\theta\hat{\theta} + B_\phi\hat{\phi}$, resulting in

$$B_\rho = B_r \sin\theta + B_\theta \cos\theta,$$
$$B_\phi = B_\phi, B_z = B_r \cos\theta - B_\theta \sin\theta. \quad (23)$$

Here, we connect the component B_ϕ with the one expressed by the circular harmonics at the reference radius ρ_{ref} [19],

$$B_\phi(\rho_{\text{ref}}, \phi) = \sum_{k=1}^{\infty}\{B_k \cos(k\phi) + A_k \sin(k\phi)\}, \quad (24)$$

where k is the order of the circular harmonics, B_k and A_k are the normal and skew components of the field harmonics at the reference radius, respectively. Noting that the term of $(\rho/\rho_{\text{ref}})^{k-1}$ in the original form is eliminated by assuming that the observed fields are located at the reference radius. Then, we make another assumption that the ratio between the reference radius ρ_{ref} and current source radius ρ' is constant everywhere along the axial direction of the magnet. Following the conical surface, the reference radius also changes linearly along the axial direction. This means that larger the conical angle is, larger the region of good field quality it has at the major radius. This also reduces the field gradient ($G = B_n/\rho_{\text{ref}}^{n-1}$) for the coil producing the high-order harmonics along the axial axis. According to the superconducting magnet design for the SuperKEKB IR [3], the quadrupole magnets nearer to the IR have stronger field gradient and smaller coil radius, and the magnets far from the IR have lower field gradient and larger bore. Currently, this assumption is practical, however, the reference region needs to be defined with the consideration of the beam optics.

In the cross section along the axial direction of the cone, the following relations are satisfied:

$$\frac{\rho_{\text{ref}}}{\rho'} = \frac{r\sin\theta}{r'\sin\beta} = \gamma,$$
$$\frac{z}{z'} = \frac{r\cos\theta}{r'\cos\beta} = 1. \quad (25)$$

The term of zenith angle can be eliminated by

$$\tan\theta = \gamma\tan\beta. \quad (26)$$

For a cone with a small conical angle, the above relation can be approximated as $\theta \approx \gamma\beta$ by considering the first-order term of the Taylor series expansion of $\tan\theta$. To simplify the calculation, we define the summation of the ALFs as

$$F_n(r) = \sum_{l=n}^{\infty}\frac{(l-n)!}{(l+n)!}P_l^n(\cos\beta)\left\{\sin\beta P_l^n(\cos\theta)S_l(r) + \cos\beta\frac{\partial P_l^n(\cos\theta)}{\partial\theta}R_l(r)\right\}. \quad (27)$$

In this function, θ can be eliminated with the relation, $\theta = \tan^{-1}(\gamma\tan\beta)$. Then, we can relate the field B_ϕ as

$$\int_0^{2\pi}\sum_{k=1}^{\infty}\{B_k\cos(k\phi) + A_k\sin(k\phi)\}\mathrm{d}\phi = -\int_0^{2\pi}\frac{\mu_0 J_n}{2}\sin\beta\cos(n\phi)F_n(r)\mathrm{d}\phi. \quad (28)$$

By taking the integration over the ϕ direction from 0 to 2π, all the terms that $k \neq n$ are removed by the orthogonality relation, and the circular harmonics can be expressed as

$$B_n(r) = -\frac{\mu_0 J_n}{2}\sin\beta F_n(r). \quad (29)$$

For a cone with a small conical angle less than 10°, the following approach is useful.

$$B_n(r) \approx -\frac{\mu_0 J_n\beta}{2} \times \sum_{l=n}^{\infty}\frac{(l-n)!}{(l+n)!}P_l^n\left(1-\frac{\beta^2}{2}\right)\left\{\beta P_l^n\left(1-\frac{\gamma^2\beta^2}{2}\right)S_l(r) + \left(1-\frac{\beta^2}{2}\right)\frac{\partial P_l^n\left(1-\frac{\gamma^2\beta^2}{2}\right)}{\partial\theta}R_l(r)\right\}. \quad (30)$$

Figure 3 shows a comparison of the main field generated by a quadrupole surface density by using the analytic form directly calculated from Eq. (29), the multipole expansion of Eq. (18), and the numerical calculation. The simulation is performed with the same cosine-theta current density at the conical surface using Finite Element Method (FEM) software, COMSOL Multiphysics®, where the magnetic field is expanded at the reference radius of $\rho_{\text{ref}} = 0.7\rho'$. The analytic form predicts reasonable circular harmonics along the axial axis, with a discrepancy for cones with large conical angles in particular. As a result of the multipole expansion of Eq. (18), the discrepancy is lowered by taking the radial component of field into account, which indicates the difference is slightly attributable to the radial field. So far, this analytic form has a good prediction for a conical coil with the angle less than 20°. Furthermore, both the analytic form and the FEM simulation show that larger conical angles result in shorter magnetic lengths because of a decrease in fields at the coil ends.

E. Field integral and magnetic length

The parameters of field integral and magnetic length play important roles in the magnetic design of accelerator magnets. We also derive the form of the field integral since

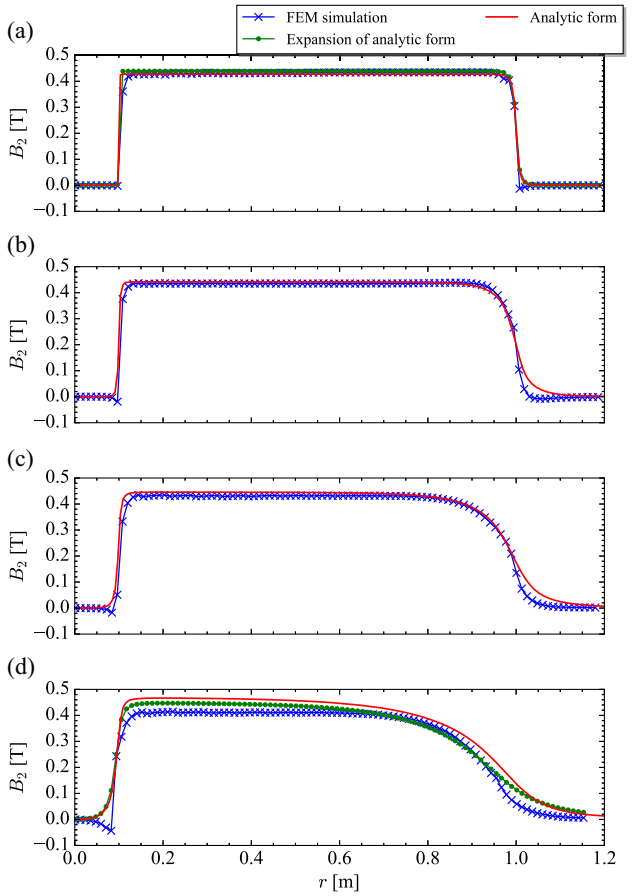


FIG. 3. The quadrupole field along the radial direction of the cone calculated by the analytic form (red line), the multipole expansion of the fields in Eq. (18) (green line), and the simulation (blue line) for different conical angles in the range of $\beta = 1° - 20°$. The coil parameters are $J_n = -10^6$ [A/m], $a = 100$ [mm], $b = 1000$ [mm], and $\gamma = 0.7$. (a) $\beta = 1°$, (b) $\beta = 5°$, (c) $\beta = 10°$, and (d) $\beta = 20°$.

the field at the coil end has a conical angle dependence. The field integral and the magnetic length are defined as

$$\tilde{B}_n = \int_0^\infty B_n(r)\mathrm{d}r, \tag{31}$$

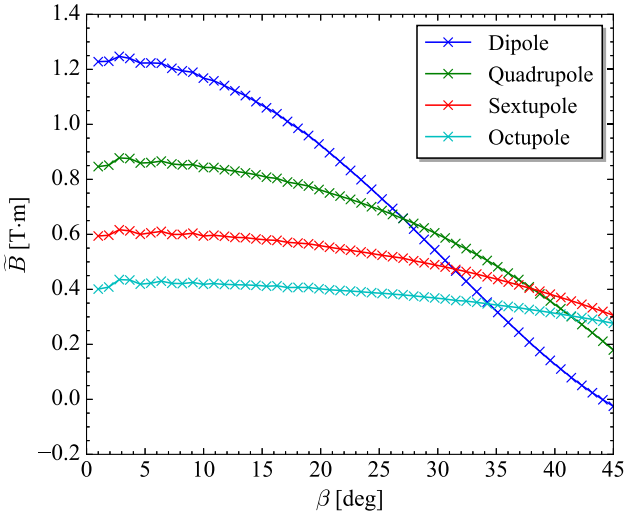


FIG. 4. The integral field for a conical dipole, quadrupole, sextupole, and octupole coil calculated by Eq. (36). The coil parameters are $J_n = -2 \times 10^6$ [A/m], $a = 10$ [mm], $b = 1000$ [mm], and $\gamma = 0.7$.

$$L = \frac{1}{B_{n,\mathrm{ref}}} \int_0^\infty B_n(r)\mathrm{d}r, \tag{32}$$

where $B_{n,\mathrm{ref}}$ is the reference main field. Substituting $B_n(r)$ with Eq. (29), the field integral can be obtained by taking the integral of the functions of $R_l(r)$ and $S_l(r)$. The integral of functions $R_l(r)$ and $S_l(r)$ can be solved as

$$\int_0^\infty R_l(r)\mathrm{d}r = (b-a)\begin{cases} 1, & l = 1 \\ \frac{1}{l} + \frac{1}{l+1}, & l \neq 1 \end{cases} \tag{33}$$

and

$$\int_0^\infty S_l(r)\mathrm{d}r = (b-a)\begin{cases} \frac{l+2}{l+1}, & l = 1 \\ \frac{1}{l} + \frac{1}{l+1} - \frac{4}{l-1}, & l \neq 1 \end{cases} \tag{34}$$

The integral of the function F_n is expressed as

$$\tilde{F}_n = \int_0^\infty F_n(r)\mathrm{d}r = (b-a)\sum_{l=n}^{\infty} \frac{(l-n)!}{(l+n)!} P_l^n(\cos\beta) \left\{ \sin\beta P_l^n(\cos\theta) \begin{cases} \frac{l+2}{l+1} \\ \frac{1}{l} + \frac{1}{l+1} - \frac{4}{l-1} \end{cases} + \cos\beta \frac{\partial P_l^n(\cos\theta)}{\partial\theta} \begin{cases} 1, & l = 1 \\ \frac{1}{l} + \frac{1}{l+1}, & l \neq 1 \end{cases} \right\} \tag{35}$$

In final, the field integral can be written as

$$\tilde{B}_n = -\frac{\mu_0 J_n}{2} \sin\beta \tilde{F}_n. \tag{36}$$

Figure 4 shows the conical angle dependence of the integral multipole fields. It can be found that the integral fields decrease as the conical angle increases because of the field drop at the major radius (see Fig. 3). With the same current, the conical coil, thereby producing high order of the field harmonics, has less conical angle dependence on the field integral. This indicates that designing a large-conical-angle dipole coil requires more current at the coil end to compensate for the field integral.

F. Current density related to field harmonics

To produce a pure field harmonics, we can take advantage of Eq. (29) and relate the current density to the field harmonics with

$$\vec{J} = -\frac{2B_n}{\mu_0 \sin\beta}\frac{1}{F_n(r')}\cos(n\phi')\hat{z}. \tag{37}$$

In this expression, we can see the current density is a function of the radius, which is not identical to the assumption of Eq. (9) that has a constant current harmonics J_n and zero divergence. Note that the axial distribution cannot be eliminated at the beginning in Eq. (10) by assuming a current density with a radial distribution, as the radial terms are coupled with the zenith angle terms in the summation.

To relate it to a constant current harmonics, we can use the average field instead of the function $F_n(\beta, \gamma; r')$ as

$$\vec{J} = -\frac{2B_n}{\mu_0 \sin\beta}\frac{1}{\bar{F}_n}\cos(n\phi')\hat{z}, \tag{38}$$

where

$$\bar{F}_n = \frac{1}{b-a}\tilde{F}_n. \tag{39}$$

Figure 5 shows the comparison of the FEM simulation results for both the surface current densities assumed in Eqs. (37) and (38), in which the target quadrupole field B_2 is assumed to be 1 T at the reference radius. Clearly, the nonconstant current harmonics increase the field at the coil end at the major radius side significantly. This approach is useful for identifying the ideal current density distribution needed to generate varying multipole harmonics along the axial direction, which is essential for shielding coil design.

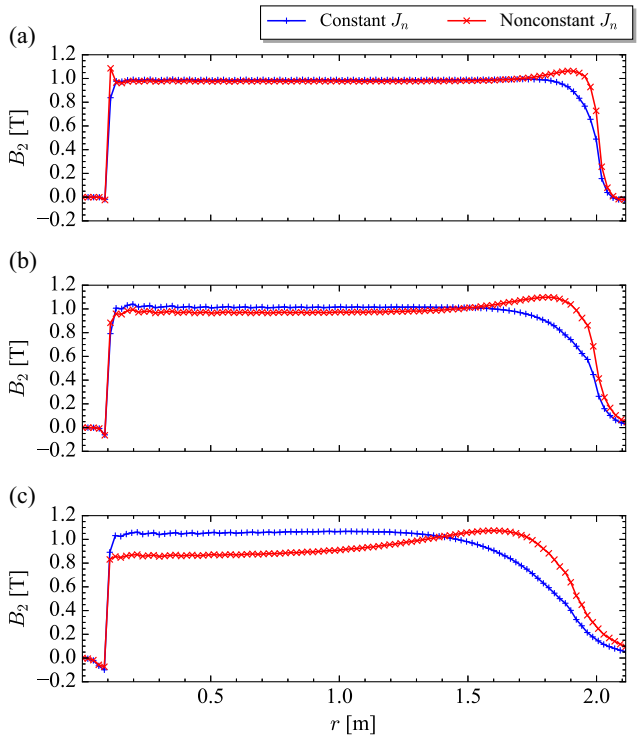


FIG. 5. The FEM simulation results calculated with the nonconstant current density (blue) and the constant current density (red) along the axial axis of the magnet. (a) $\beta = 5°$, (b) $\beta = 10°$, and (c) $\beta = 20°$.

III. CONICAL CANTED-COSINE-THETA COIL

In this section, we present a method for generating the winding path for a CCT conical coil, leveraging the techniques proposed in [20,21]. Subsequently, we verify the magnetic field produced by a pair of the conical CCT windings using the Biot-Savart law.

A. Single layer CCT winding path

Based on the field established in the previous section, the fields and circular harmonics of the conical coil can be derived from the spherical coordinate system. Thus, the CCT winding path is constrained to the surface of a sphere intersected by a constant conical angle β. The path is parameterized as a function of azimuthal angle ϕ

$$r = p_r(\phi), \qquad \theta = \beta, \qquad \phi = \phi, \tag{40}$$

where $p_r(\phi)$ is a yet undefined path function which describes the axial movement along the conical surface. A local reference frame at location $\vec{p}(\phi) = p_r(\phi)\hat{r}$ is defined for the winding path as illustrated in Fig. 6. Here, $\hat{n}$ is the unit normal vector which is normal to $\hat{\theta}$, $\hat{t}$ is the unit vector tangential to the path, and $\hat{b}$ is the unit binormal vector.

The tangential vector to the path can be found to be

$$\vec{t} = \frac{d\vec{p}}{d\phi} = p_r(\phi)\sin\beta\hat{\phi} + p_r'(\phi)\hat{r}, \tag{41}$$

where $p_r'(\phi)$ is the derivative of path at the given ϕ. Given that $\hat{\theta}$ is the normal vector of the conical surface, we can

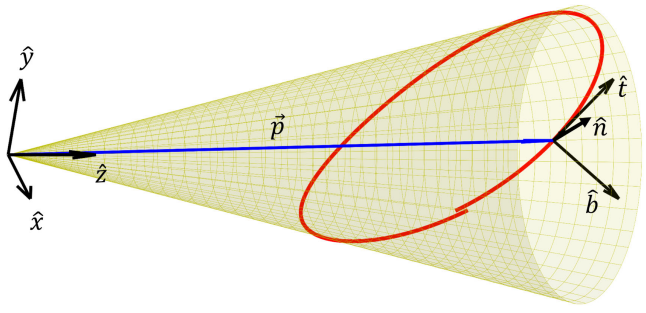


FIG. 6. Definition of the CCT path vector $\vec{p}$ and the local unit coordinate $(\hat{t}, \hat{b}, \hat{n})$.

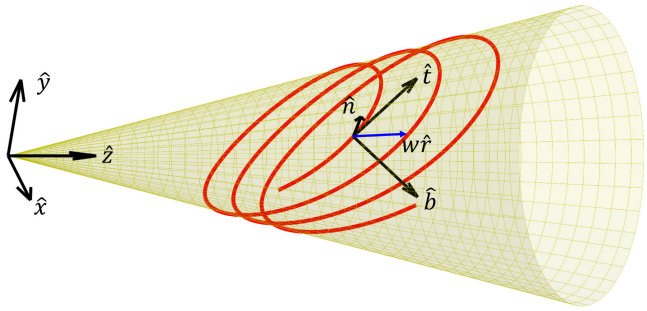


FIG. 7. The periodic winding path with the pitch length of w in the spherical coordinate.

obtain the unit binormal vector of $\hat{b}$ by taking the cross product of the tangential vector and $\hat{\theta}$ as

$$\vec{b}(\phi) = \vec{t} \times \hat{\theta} = -p_r(\phi)\sin\beta\hat{r} + p_r'(\phi)\hat{\phi}. \tag{42}$$

To relate the current density to the winding, we assume the CCT coil is wound with a pitch, w, pointing in the radial direction, as shown in Fig. 7. Using the unit binormal vector of the winding path, the distance between adjacent turns is represented as

$$\delta(\phi) = w\hat{r}\cdot\hat{b} = \frac{wp_r(\phi)\sin\beta}{\sqrt{p_r^2(\phi)\sin^2\beta + p_r'^2(\phi)}}. \tag{43}$$

Then, we can average the operating current with the above distance between adjacent turns; and the averaged current density can be represented as

$$\vec{J}(\phi) = \frac{I\hat{t}}{\delta(\phi)} = \frac{I}{wp_r(\phi)\sin\beta}\{p_r(\phi)\sin\beta\hat{\phi} + p_r'(\phi)\hat{r}\}, \tag{44}$$

where I is the operating current in the winding path. The current density of the CCT winding path only has radial and azimuthal components, where the radial component can be connected to the field harmonics of the cosine-theta current density assumed in Eq. (9) as

$$\frac{I}{wp_r(\phi)\sin\beta}\{p_r(\phi)\sin\beta\hat{\phi} + p_r'(\phi)\hat{r}\} = J_n\cos(n\phi)\sin\beta\hat{r} - J_n\cos(n\phi)\cos\beta\hat{\theta}. \tag{45}$$

Taking the integration of both sides, we obtain the following differential equation:

$$\int\frac{dp_r}{p_r} = \frac{J_n w}{I}\sin^2\beta\int\cos(n\phi)d\phi. \tag{46}$$

Unlike the CCT winding, which has a constant radius, the radius of the conical CCT changes to a function of azimuthal angle ϕ, which leads to the solution with the exponential function.

Note that the winding path starts at the minor radius, and the winding is repeated after one turn. Therefore, the following initial and periodic conditions must be input into Eq. (46) to solve the winding path:

$$p_r(0) = a, \tag{47}$$

$$|p_r(\phi + 2\pi) - p_r(\phi)| = w. \tag{48}$$

Applying above conditions, we obtain the path function and its derivative as

$$p_r(\phi) = \left(a + \frac{w}{2\pi}\phi\right)\exp\left\{\frac{J_n w}{I}\frac{\sin^2\beta}{n}\sin(n\phi)\right\},$$
$$p_r'(\phi) = \frac{p_r(\phi)}{\frac{2\pi a}{w} + \phi} + \frac{J_n w}{I}p_r(\phi)\sin^2\beta\cos(n\phi), \tag{49}$$

where the range of ϕ is determined as $0 < \phi \le 2N\pi$, and $N = \frac{b-a}{w}\cos\beta$ is the number of the turns corresponding to the number of the CCT loops.

Furthermore, the current density and the operating current can be represented by a tilt angle α as

$$\tan\alpha = \left.\frac{\vec{t}\cdot\hat{\phi}}{\vec{t}\cdot\hat{r}}\right|_{\phi=0,a=0} = \frac{I}{J_n w\sin\beta}. \tag{50}$$

Using the current density derived in Eq. (37) or Eq. (38), we can determine the tilt angle related to the desired multipole field as

$$\tan\alpha = -\frac{\mu_0 I}{2B_n}\frac{F_n(r)}{w\sin\beta} \tag{51}$$

$$= -\frac{\mu_0 I}{2B_n}\frac{\bar{F}_n}{w\sin\beta}. \tag{52}$$

As $F_n(r)$ depends on the axial position r, this is useful for designing shielding coils with harmonic profiles. Finally, the parameterized winding path and its derivative for a CCT on the conical surface are given by

$$p_r(\phi) = \left(a + \frac{w}{2\pi}\phi\right)\exp\left\{\frac{\cot\alpha}{n}\sin\beta\sin(n\phi)\right\},$$
$$p_r'(\phi) = p_r(\phi)\left\{\frac{1}{\frac{2\pi a}{w} + \phi} + \cot\alpha\sin\beta\cos(n\phi)\right\}. \tag{53}$$

The winding path in the Cartesian coordinate is given by

$$x = p_r(\phi)\sin\beta\cos\phi$$
$$y = p_r(\phi)\sin\beta\sin\phi \quad . \tag{54}$$
$$z = p_r(\phi)\cos\beta$$

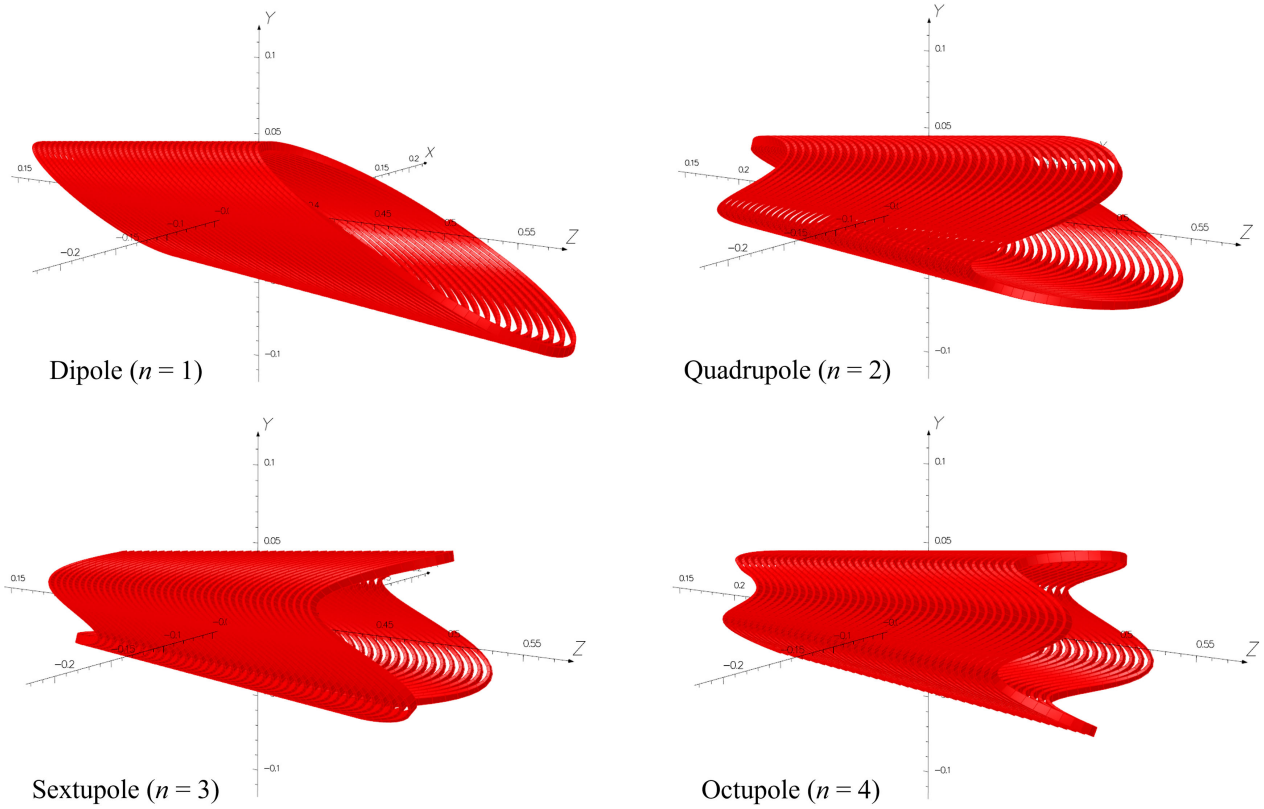


FIG. 8. Single conical CCT winding for producing the dipole ($n = 1$), quadrupole ($n = 2$), sextupole ($n = 3$), and octupole ($n = 4$) fields.

As an example, the single layer of conical CCT windings with a conical angle of $\beta = 5°$ and a constant tilt angle of 20° produced by the above formula is shown in Fig. 8.

The vector of the current density for a single layer of the CCT winding is given by

$$\vec{J}(\phi) = \frac{I}{w}\hat{\phi} + \left\{\frac{I}{\sin\beta(2\pi a + w\phi)} + \frac{I}{w}\cot\alpha\cos(n\phi)\right\}\hat{r}. \tag{55}$$

Even if we assume the surface current density is flowing along the z direction, only the azimuthal and radial components remain, which generate a solenoid field and transverse field, respectively. Appendix gives the expression related to the radial current density. According to the CCT concept, the solenoid field and the field generated by the winding pitch can be canceled by an additional layer of CCT winding with a negative tilt angle and operating current. Furthermore, the additional layer also doubles the main multipole field. Since the radial component of the current density is decomposed to the field component B_z, this component B_z cannot be canceled out by the additional layer.

B. Multilayer conical CCT

To cancel the unwanted fields, another layer of single CCT winding with the same conical angle β is needed. Since the radius of the cone and its axial location can be expressed in the spherical coordinate system as $\rho = a\sin\beta$ and $z = a\cos\beta$, we generate the second layer with the same conical angle and a larger conical radius and then shift the winding path along the axial direction with the offset of

$$\Delta z = z_2 - z_1 = (\rho_{0,2} - \rho_{0,1})\cot\beta, \tag{56}$$

where $\rho_{0,1}$ and $\rho_{0,2}$ are the minor radius of the first and second layers, respectively. Figure 9 illustrates a pair of single conical CCT layer assembled together. The second

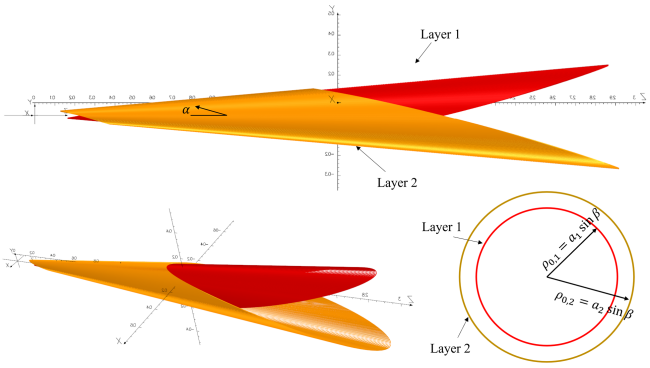


FIG. 9. A pair of conical CCT windings. The solenoid field generated by the first layer is canceled out by the second layer. The minor radius of the first and second layers are $\rho_{0,1}$ and $\rho_{0,2}$, respectively.

TABLE I. Parameters for producing the conical CCT winding.

Item	Unit	Value
Pole, n		1, 2
Winding pitch, w	mm	6
Minor radius (first layer), $\rho_{0,1}$	mm	20
Minor radius (second layer), $\rho_{0,2}$	mm	30
Conical angle, β	deg	5
Total turns, N		300
Operating current, I	A	2000
Tilt angle, α	deg	20
Reference radius factor, γ		0.7
Length, h	m	1.8

layer is slightly longer than the first layer. The offset assumes that the start points of the first and second layers are aligned at the same axial position. In practice, the offset and the tilt angle of the second layer can be modified to obtain the desired magnetic field quality.

Assuming the CCT magnet has identical intervals for each layer, the offset at ith layer is given by

$$\Delta z_i = (i-1)\delta\rho\cot\beta, \qquad (i = 1, 2, \ldots, N_{ly}), \tag{57}$$

where $\delta\rho$ is the distance between the two adjacent layers, and N_{ly} is the number of CCT layers.

C. Magnetic field of the conical CCT coils

Here, we perform a dipole and quadrupole conical CCT design to verify the winding path and its field qualities. Both the dipole and the quadrupole coils are produced with the coil parameters listed in Table I. The coil only contains a pair of CCT windings connected in series, and the interval between the first and the second layer is assumed to be 10 mm. The reference radius $\rho_{\mathrm{ref}} = \gamma z\tan\beta$ is changed along the axial direction, scaled from the inner radius of the winding by a factor of 0.7.

Figure 10 shows the axial multipole fields calculated by the Biot-Savart law, and their integral field harmonics are listed in Table II. The results indicate that the coils have a very flat main field distribution in the region where the first layer is fully covered by the second layer. A dramatic field decay at the coil ends is proportional to the CCT tilt angle, as the larger tilt angle results in a longer winding tail. A smaller tilt angle provides a shorter field decay region, but it also reduces the main multipole field.

The coil end also creates peaks of field error corresponding to the orders of $n+2$, where n is the main field. For the application of accelerator magnets, despite these large field errors, they are symmetrical and can be canceled out by integration, which may not significantly affect the beam dynamics.

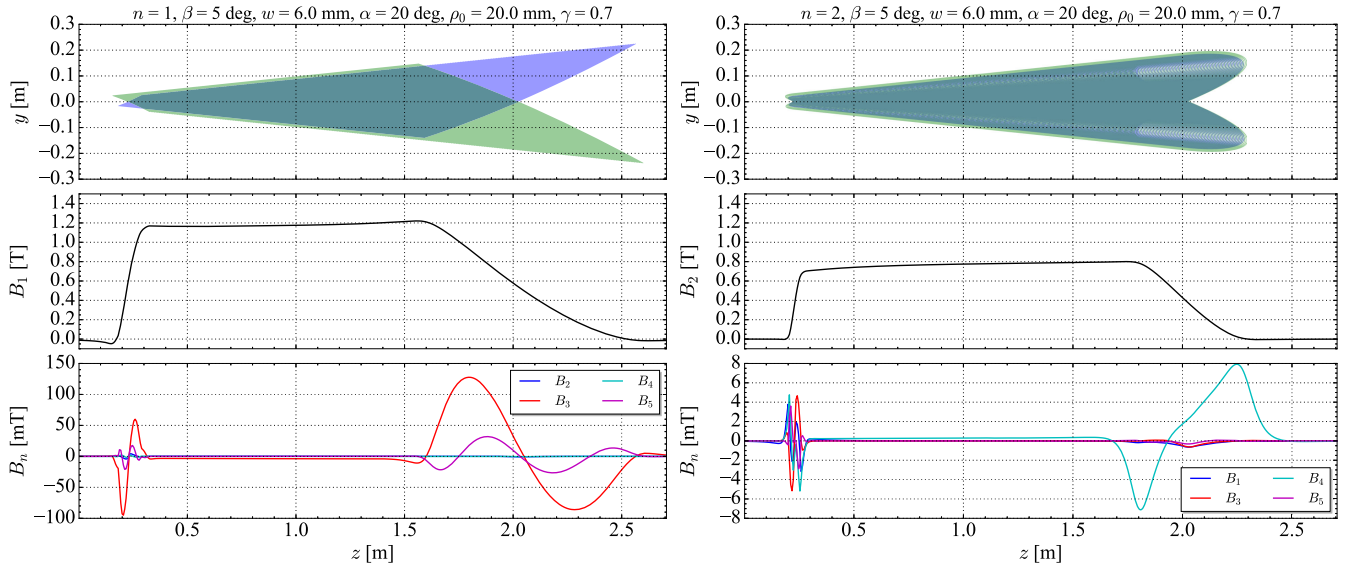


FIG. 10. Multipole fields produced by a dipole (left) and quadrupole (right) conical CCT coils along the axial direction. The black line indicate the main field. The reference radius is assumed to be a function of $\rho_{\mathrm{ref}}(z) = \gamma z\tan\beta$.

TABLE II. Integral field harmonics for the dipole and quadrupole conical CCT. The field at the cone center $z = z_0 + h/2$ is treated as the main field.

Item	Unit	Value					
Coil type		Dipole			Quadrupole		
Main field	T	1.2			0.8		
Magnetic length	m	1.74			1.71		
Layer		1	2	All	1	2	All
$\tilde{B}_1$	T · m	1.03	1.06	2.10	-1.25×10^{-4}	-1.43×10^{-5}	-1.39×10^{-4}
$\tilde{B}_2$	T · m	-1.90×10^{-5}	2.34×10^{-4}	2.15×10^{-4}	0.72	0.66	1.38
$\tilde{B}_3$	T · m	9.37×10^{-4}	1.33×10^{-3}	2.27×10^{-3}	-3.90×10^{-5}	-3.94×10^{-5}	-7.84×10^{-5}
$\tilde{B}_4$	T · m	-2.65×10^{-4}	-8.08×10^{-5}	-1.07×10^{-4}	6.51×10^{-4}	7.16×10^{-4}	1.37×10^{-3}
$\tilde{B}_5$	T · m	-2.24×10^{-5}	2.84×10^{-5}	6.04×10^{-6}	-1.49×10^{-5}	-1.33×10^{-5}	-2.82×10^{-5}
$\tilde{B}_6$	T · m	-1.28×10^{-5}	1.17×10^{-6}	-1.16×10^{-5}	-2.11×10^{-5}	-2.23×10^{-5}	-4.34×10^{-5}

IV. CONCLUSION

This paper presents the analytic expression of producing the magnetic field for a finite, long, conical coil. We solved the magnetic fields generated by a conical surface carrying a general cosine-theta current density along the radial direction in the spherical coordinate system. Then, we relate the magnetic fields to the circular field harmonics which allowed us to determine the current density distribution required for specific field harmonics. Finally, the method was applied to a CCT design, and we provided a formula to produce a conical CCT coil with the required field harmonics.

The method developed in this paper enables determination of the winding path with the required field harmonics for a finite long conical CCT coil. This advancement has potential applications in the interaction regions of high-energy particle colliders and scanning magnets for radiotherapy accelerators.

ACKNOWLEDGMENTS

This work was supported by the Director, Office of 609 Science, High Energy Physics, and U.S. Department of 610 Energy Under Contract No. DE-AC02-05CH11231. The authors acknowledge Jose Luis Rudeiros Fernandez and Paolo Ferracin of Lawrence Berkeley National Laboratory for feedback on this work and interesting discussions on the conical CCT magnet.

DATA AVAILABILITY

The data are not publicly available. The data are available from the authors upon reasonable request.

APPENDIX: MAGNETIC FIELD PRODUCED BY THE RADIAL CURRENT DENSITY

We start from a current density with both the radial and azimuthal components in this study. However, the azimuthal component just disappears when the CCT path is related to the ideal current density, as given in Eq. (45). Here, we start from the following current density and give a solution of the magnetic field produced by the radial component of the current density.

$$\vec{J} = J_n \cos(n\phi')\hat{r}. \tag{A1}$$

The vector potential can be obtained with the same procedure described in Sec. II as

$$A_r(r,\theta,\phi) = \frac{\mu_0 J_n}{2} r \sin\beta \cos(n\phi) \sum_{l=n}^{\infty} \frac{(l-n)!}{(l+n)!} P_l^n(\cos\beta) P_l^n(\cos\theta) R_l(r). \tag{A2}$$

Each component of the magnetic fields are accordingly written as

$$B_\theta(r,\theta,\phi) = -\frac{\mu_0 J_n}{2} \sin\beta \sin(n\phi) \sum_{l=n}^{\infty} \frac{(l-n)!}{(l+n)!} P_l^n(\cos\beta) \frac{n P_l^n(\cos\theta)}{\sin\theta} R_l(r), \tag{A3}$$

$$B_\phi(r,\theta,\phi) = -\frac{\mu_0 J_n}{2} \sin\beta \cos(n\phi) \sum_{l=n}^{\infty} \frac{(l-n)!}{(l+n)!} P_l^n(\cos\beta) \frac{\partial P_l^n(\cos\theta)}{\partial\theta} R_l(r). \tag{A4}$$

Using the relation in Eq. (26), the multipole field along the radial axis is given by

$$B_n(r) = -\frac{\mu_0 J_n \sin\beta}{2} \sum_{l=n}^{\infty} \frac{(l-n)!}{(l+n)!} P_l^n(\cos\beta) \frac{\partial P_l^n(\cos\theta)}{\partial\theta} R_l(r). \tag{A5}$$

The integral multipole field is

$$\tilde{B}_n = -\frac{\mu_0 J_n (b-a) \sin\beta}{2} \sum_{l=n}^{\infty} \frac{(l-n)!}{(l+n)!} P_l^n(\cos\beta) \frac{\partial P_l^n(\cos\theta)}{\partial\theta} \begin{cases} 1, & l=1 \\ \frac{1}{l-1} + \frac{1}{l+2} + \frac{1}{(l+1)(l+2)} - \frac{1}{(l-1)l}, & l \neq 1 \end{cases}. \tag{A6}$$

[1] H. Witte *et al.*, The interaction region of the electron-ion collider EIC, in *Proceedings of the 12th International Particle Accelerator Conference, IPAC-2021, Campinas, SP, Brazil* (JACoW, Geneva, Switzerland, 2021), pp. 2574–2577, https://proceedings.jacow.org/ipac2021/doi/JACoW-IPAC2021-WEPAB002.html.

[2] M. Koratzinos, The FCC-ee interaction region magnet design, in *Proceedings of eeFACT2016, Daresbury, UK* (2016), pp. 57–60, arXiv:1607.05446.

[3] N. Ohuchi *et al.*, SuperKEKB beam final focus superconducting magnet system, Nucl. Instrum. Methods Phys. Res., Sect. A **1021**, 165930 (2022).

[4] B. Parker *et al.*, Superconducting corrector IR magnet production for SuperKEKB, in *Proceedings of the 4th International Particle Accelerator Conference, IPAC-2013, Pasade, Shanghai, China* (JACoW, Geneva, Switzerland, 2013), pp. 1241–1243.

[5] B. Parker *et al.*, The SuperKEKB interaction region corrector magnets, in *Proceedings of International Particle Accelerator Conference, IPAC-2016, Busan, Korea* (JACoW, Geneva, Switzerland, 2016), pp. 1193–1195.

[6] B. Parker *et al.*, Test of a model superconducting magnet for the HERA ep interaction regions, IEEE Trans. Appl. Supercond. **10**, 272 (2000).

[7] P. Wanderer *et al.*, Completion of superconducting magnet production at BNL for the HERA luminosity upgrade, IEEE Trans. Appl. Supercond. **12**, 305 (2002).

[8] D. Meyer and R. Flasck, A new configuration for a dipole magnet for use in high energy physics applications, Nucl. Instrum. Methods **80**, 339 (1970).

[9] S. Caspi *et al.*, Canted-cosine-theta magnet (CCT)—A concept for high field accelerator magnets, IEEE Trans. Appl. Supercond. **24**, 4001804 (2014).

[10] H. Witte, B. Parker, and R. Palmer, Design of a tapered final focusing magnet for eRHIC, IEEE Trans. Appl. Supercond. **29**, 4004105 (2019).

[11] P. Xu, H. Witte, S. Notaro, and Y. Bai, Structural analysis of multilayer tapered canted-cosine-theta superconducting magnet for the interaction region of electron ion collider, IEEE Trans. Appl. Supercond. **35**, 4101405 (2019).

[12] QST and Toshiba achieve major breakthrough in greatly downsizing pencil beam scanning system for heavy-ion therapy, https://www.qst.go.jp/soshiki/4/1077.html (2018).

[13] Y. Iwata *et al.*, Design of a superconducting rotating gantry for heavy-ion therapy, Phys. Rev. ST Accel. Beams **15**, 044701 (2012).

[14] Y. Iwata *et al.*, Design of a compact superconducting accelerator for advanced heavy-ion therapy, Nucl. Instrum. Methods Phys. Res., Sect. A **1053**, 168312 (2023).

[15] T. Miyatake *et al.*, Design study of conical-canted-cosine-theta scanning magnet for heavy ion therapy, IEEE Trans. Appl. Supercond. (to be published).

[16] S. Caspi, L. Brouwer, L. G. Fajardo, and Y. Yang, A conical accelerator magnet with unique CCT properties, IEEE Trans. Appl. Supercond. **35**, 4100504 (2025).

[17] J. D. Jackson, *Classical Electrodynamics* (John Wiley & Sons, Inc., New York, 2007).

[18] M. Eshagh, Non-singular expressions for the vector and the gradient tensor of gravitation in a geocentric spherical frame, Comput. Geosci. **34**, 1762 (2008).

[19] K. H. Mess, S. Wolff, and P. Schmuser, *Superconducting Accelerator Magnets* (World Scientific, Singapore, 1996).

[20] L. Brouwer, Producing circular field harmonics inside elliptic magnet apertures with superconducting canted-cosine-theta coils, Phys. Rev. Accel. Beams **27**, 022402 (2024).

[21] L. Brouwer, Canted-cosine-theta superconducting accelerator magnets for high energy physics and ion beam cancer therapy, Ph.D. Thesis, University of California, Berkeley, 2015.